warwick.ac.uk/lib-publications

An Evaluation of Silicon Carbide Unipolar Technologies for Electric Vehicle Drive-trains

Saeed Jahdi, *Member, IEEE,* Olayiwola Alatise, *Member, IEEE,* Craig Fisher, *Member, IEEE,*
Li Ran, *Senior Member, IEEE,* and Philip Mawby, *Senior Member, IEEE*

Abstract—Voltage Sourced Converters (VSC) in electric vehicle drive-trains are conventionally implemented by silicon IGBTs and PiN diodes. The emergence of SiC unipolar technologies opens up new avenues for power integration and energy conversion efficiency. This paper presents a comparative analysis between 1.2 kV SiC MOSFET/Schottky diodes and silicon IGBT/PiN diode technologies for electric vehicle drive-train performance. The switching performances of devices have been tested between -75 $^\circ$C and 175 $^\circ$C at different switching speeds modulated by a range of gate resistances. The temperature impact on the electromagnetic oscillations in SiC technologies and reverse recovery in silicon bipolar technologies is analyzed, showing improvements with increasing temperature in SiC unipolar devices whereas those of the silicon-bipolar technologies deteriorate. The measurements are used in an EV drive-train model as a 3-level Neutral Point Clamped (NPC) VSC connected to an electric machine where the temperature performance, conversion efficiency and the Total Harmonic Distortion (THD) is studied. At a given switching frequency, the SiC unipolar technologies outperform silicon bipolar technologies showing an average of 80% reduction in switching losses, 70% reduction in operating temperature and enhanced conversion efficiency. These performance enhancements can enable lighter cooling and more compact vehicle systems.

Index Terms—Power Semiconductor Devices, Silicon Carbide, Electric Vehicles, Switching Circuits, Pulse Width Modulation Converters.

I. INTRODUCTION

POWER electronics for electric vehicle drive-trains is essential for high efficiency energy conversion [1], [2] . Transiting from slow switching silicon bipolar to fast switching SiC unipolar technologies is expected to imporve the performance and efficiency of electric vehicles (EV) [3]. Silicon carbide technology has increased the voltage range of MOSFETs. The wide bandgap and higher critical electric field means that higher voltages can be blocked with thinner and more conductive epitaxial layers. The higher thermal conductivity will make them more temperature rugged and the wider bandgap means less leakage currents and reduced probability of thermal runaway in high temperature applications. As a result 1.2 kV SiC MOSFETs and Schottky diodes have been manufactured by CREE and ROHM (amongst others) with very low conduction losses and are now commercially available. SiC MOSFETs with blocking voltages as high as 10 kV [4]–[6] and with increasingly higher currents have also been demonstrated [7]. The feasibility of SiC technology for energy conversion in fully rated power converters for wind turbine energy conversion and fuel-cell systems was explored in [8], [9] and the implementation of SiC devices in motor control drive-trains has been explored in [10]. The impact of SiC unipolar devices on the system level performance of hybrid electric vehicle power-trains was investigated in [11], where it was seen that system efficiency as well as compactness was improved. The use of SiC devices in an on-board electric vehicle battery charger was also investigated in [12] with results showing improved efficiency.

The goal of this paper is to investigate the impact of SiC unipolar devices in electric vehicles through both simulations and experimental characterization of switching transients. To ensure high fidelity of model results, the power device switching models in the converter have been parameterized by extensive experimental measurements over a wide range of temperatures (-75 $^\circ$C and 175 $^\circ$C) and switching rates. The temperature dependency of the current and voltage transients will be analyzed and the impact of the switching rate on voltage oscillations and reverse recovery will be discussed. 1.2 kV SiC MOSFETs and Schottky diodes are compared with similarly rated Silicon IGBTs and PiN diodes and a 3-level 3-phase NPC voltage source converter is used together with a PMSM motor model to emulate the EV drive-train. Section II presents the experimental test set-up and preliminary measurement results, Section III discusses the temperature behavior of the power devices, Section IV discusses the EV drive-train models while Section V concludes the paper.

II. CLAMPED INDUCTIVE SWITCHING MEASUREMENTS

Figure 1 shows circuit schematic of the clamped inductive switching test rig using a standard double-pulse method while Figure 2 shows the picture of the experimental set-up designed for this purpose. The SiC MOSFETs are ROHM devices (SCH2080KE) rated 35 A at T_C=25 $^\circ$C and 22 A at T_C = 100 $^\circ$C whereas the SiC diodes are Semisouth

SDP30S120 rated as 46 A at $T_C < 100\,°C$. The IGBTs are IXYS IXDH20N120D1 (NPT technology) rated as 38 A at $T_C = 25\,°C$ and 25 A at $T_C = 90\,°C$ and the PiN diodes are IXYS DSI45-12A rated as 45 A at $T_C = 130\,°C$. The values of the components in the test rig and parameters used in both model and practical experiments are in Table I. The testing is done using standard double-pulse method. The low-side transistor is switched on to charge the inductor to a pre-defined current level. When the transistor is switched off, the current commutates to the diode and free-wheels, after which the transistor is switched on again.
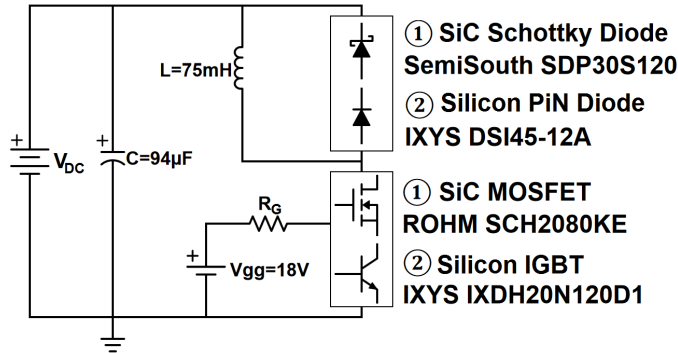

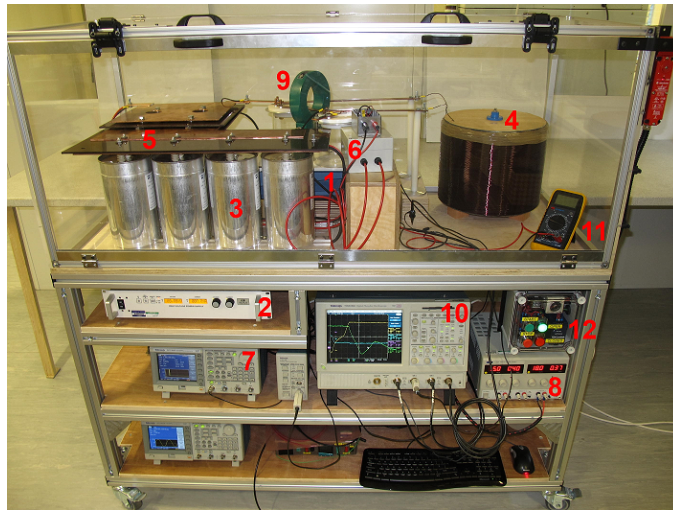Fig. 1. Quasi-Switching Clamped Inductive Test Rig Schematic

Fig. 2. HV Test Rig Components: 1- Thermal Conditioner 2- 12 kV Power Supply 3- 6.5 kV Bank Capacitors 4- 75mH Inductor 5- Copper Plates 6- Gate Driver 7- Signal Generator 8-Gate Supply 9-Current Probe 10- Oscilloscope 11-Voltmeter 12- Interlock

The circuit forces current commutation between the transistor and diode and is able to test the switching energies of the transistors and diodes. Transistor switching is performed with a range of gate resistors from 10 Ω to 1000 Ω (with an incrementally increase on a logarithmic basis) correlating with turn-ON dI_{DS}/dt ranging from 10 A/μs to 400 A/μs [13]. The wide range of gate resistances was selected so as to ensure sufficient measurement information was obtained for investigating phenomena like the temperature dependency of the switching rate, the dependency of the diode oscillation frequency (for SiC Schottky) and reverse recovery (for Silicon

PiN) on the switching rate. Figure 3 shows the general classic double pule testing waveforms. Figure 4(a) shows the voltage turn-ON characteristics of devices switched with a gate resistance, $R_G = 15$ Ω whereas Figure 4(b) shows the current turn-ON characteristics. Figure 4(c) shows the voltage turn-ON characteristics of the devices switched with $R_G = 150$ Ω whereas Figure 4(d) shows the current turn-ON characteristics. Both devices are switched at 1 kV at room temperature under identical conditions. Figure 5(a) to 5(d) show the corresponding plots for turn-OFF.
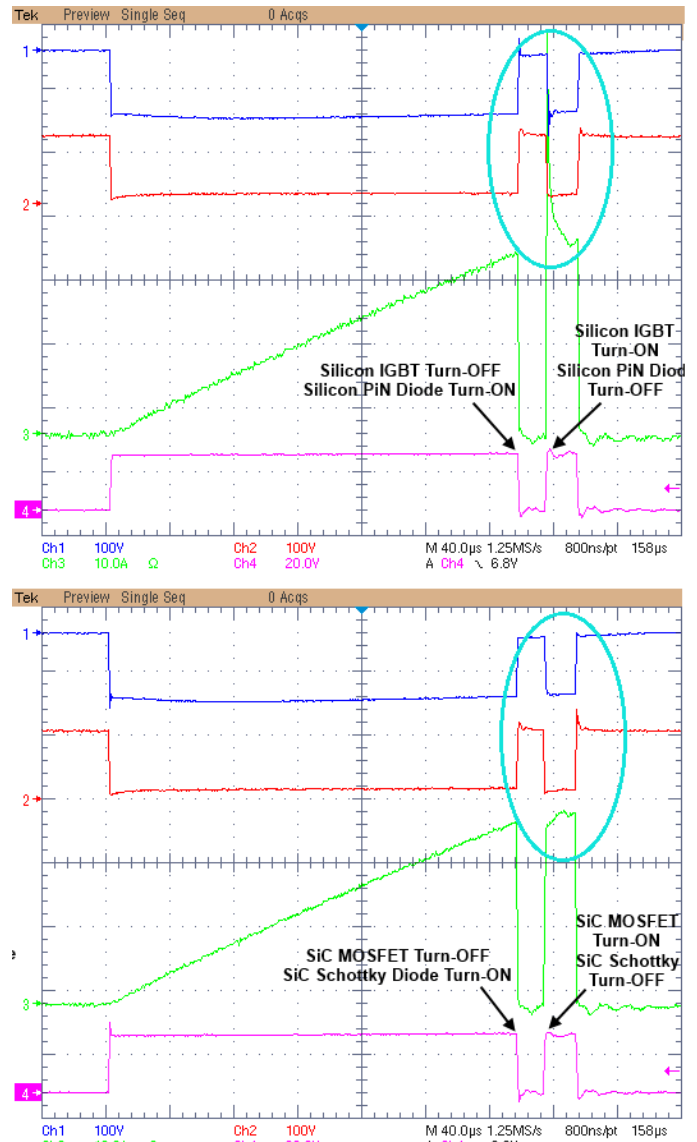
Fig. 3. Double-pulse clamped inductive measurements for Top: Silicon devices, Bottom: SiC devices

Figure 6 shows the switching energy for all gate resistances for the silicon IGBT and the SiC MOSFET where it can be seen that the SiC MOSFET exhibits 80% less switching energy on average. Figure 7 shows the switching energy as a function of the drain/collector voltage on the DC bus. The switching energy has been normalized by the current so it is presented in mJ per Amp.

TABLE I
TESTS PARAMETERS, UNITS AND THEIR VALUES

| Symbol	Elucidation	Values
T	Temperature Range	-75 °C to 175 °C
R_G	Gate Resistances Range	10 Ω to 1000 Ω
L	Total inductance of the test rig inductors	75 mH
C	Total capacitance of the bank capacitors	94 μF
C_{DC}	Converter DC link capacitor (each)	320 μF
V_{DC}	Source DC-Voltage	100-1000 V
V_{PP}	Peak voltage on devices (as overshoot)	1120 V
I_{DC}	Source DC-Current	125 mA
I_{PP}	Peak current on devices after the Inductive/Capacitive banks	30 A
R_{th}	Thermal resistance of the heat sink in converter (from datasheet)	0.32 m^{2}K/W
C_{th}	Thermal capacitance of the heat sink in converter (from datasheet)	3.93 J/K
t_{Q1}	Duration of quasi inductive signal	250 μs
t_{Q2}	Duration of gate switching signal	20 μs
V_{gg}	Gate Voltage	18 V
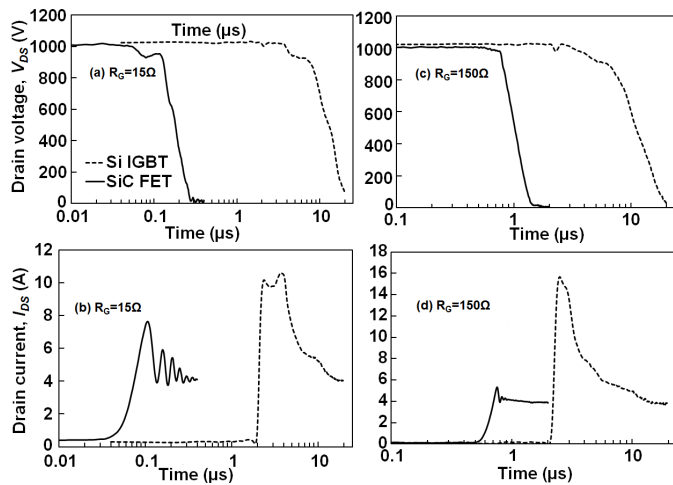
Fig. 4. Turn-ON waveforms of Silicon IGBT / SiC MOSFET with 15 Ω and 150 Ω gate resistances respectively at 1kV voltage rating
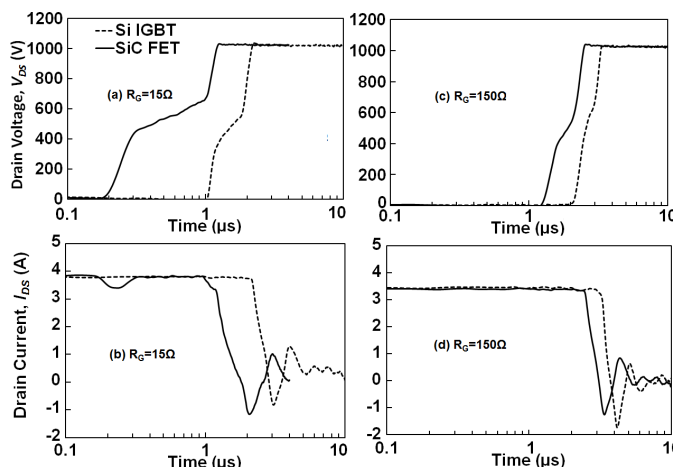

Fig. 5. Turn-OFF waveforms of Silicon IGBT / SiC MOSFET with 15 Ω and 150 Ω gate resistance respectively at 1kV voltage rating

Figure 7 shows that the switching energy increases linearly with the DC voltage for both devices at turn-OFF and ON. The improved performance of the SiC transistors is extended to all voltages. In the following section, switchings are assessed between -75 °C and 175 °C.
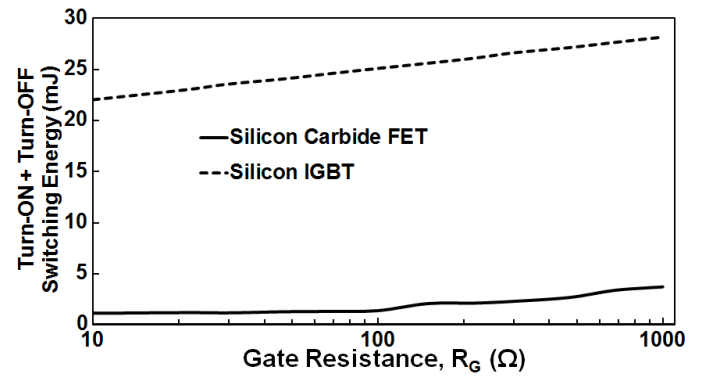
Fig. 6. Switching energy as a function of the gate resistance for the SiC MOSFET and Silicon IGBT showing significantly better performance of the SiC MOSFET, test is performed at 25 °C and 1 kV
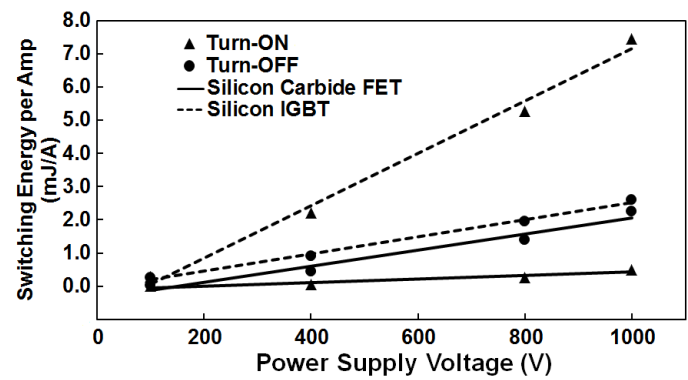
Fig. 7. Switching energy per Amp of Silicon IGBT/SiC MOSFET following a linear trend on a range of voltages tested up to 1kV with R_G=15 Ω at 25 °C

III. TEMPERATURE DEPENDENCY OF SWITCHING ENERGY

The switching energies of the transistors and diodes have been calculated at turn-ON and turn-OFF over a wide temperature and dI_{DS}/dt range. The temperature is varied by placing the devices in a thermal chamber while the dI_{DS}/dt is varied by using different gate resistors. The initial operating temperature has been set by the environmental chamber housing the devices. Before performing each test, sufficient time has been given so as to allow the devices attain equilibrium with the ambient temperature. It should be noted that the ambient temperature, which is set by the chamber, is not equal to the junction temperature during switching since there will be additional self-heating from the transistors and diodes. Hence, the junction temperatures of the devices will be higher. SiC devices also have lower conduction losses due to thinner and less resistive voltage blocking epitaxial layers compared with silicon unipolar devices. This means self-heating will be less.

One of the main advantages that SiC unipolar devices provide is that their ability to provide faster switching transients as well as lower conduction losses due to smaller on-state resistance ($R_{DS_{ON}}$). This is unlike IGBTs where low conduction losses usually come at the price of long current tails, for example punch-through IGBTs. The IGBTs used in this experiment is of non-punch-through (NPT) technology with smaller current tails compared to punch-through (PT) IGBTs.

A. Transistor Turn-ON

Figure 8 shows the turn-ON switching energy of the SiC MOSFET as a function of the dI_{DS}/dt determined by the gate resistance) and temperature. It can be seen from Figure 8 that the best turn-ON performance of the SiC MOSFET is when it is driven fast and hot. The switching energy decreases with increasing temperature and dI_{DS}/dt (decreasing R_G). The negative temperature coefficient of the switching energy in the SiC MOSFET is due to the fact that dI_{DS}/dt increases with temperature during turn-ON. This can be seen in Figure 9 and Figure 10 where the turn-ON voltage and current transients are shown at different temperatures for the 15 Ω and 150 Ω switching respectively.
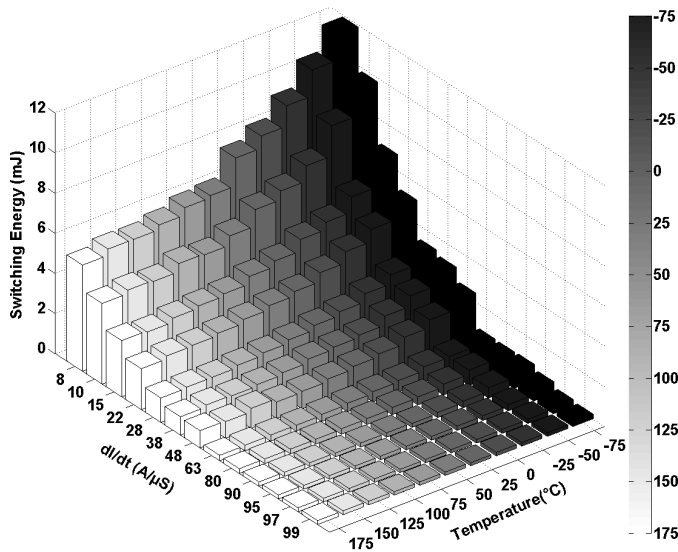

Fig. 8. Switching energy of SiC MOSFET at turn-ON

Higher dI_{DS}/dt generally reduces the duration of the switching transient, thereby reducing the switching energy since the latter is the integration of the switching power over the switching time. The rate of change of the dI_{DS}/dt with temperature increases for the larger gate resistances hence; there is greater variation of switching energy with temperatures dI_{DS}/dt as is reduced. For example, at turn-ON of SiC MOSFET in R_G=15 Ω (Figure 8), the switching energy decreases by 20% when the temperature is increased from -75 °C to 175 °C, whereas at R_G=1000 Ω, the switching energy decreases by 50% for the same range of temperature change.

Fig. 9. SiC MOSFET turn-ON voltage and current with an R_G of 15 Ω
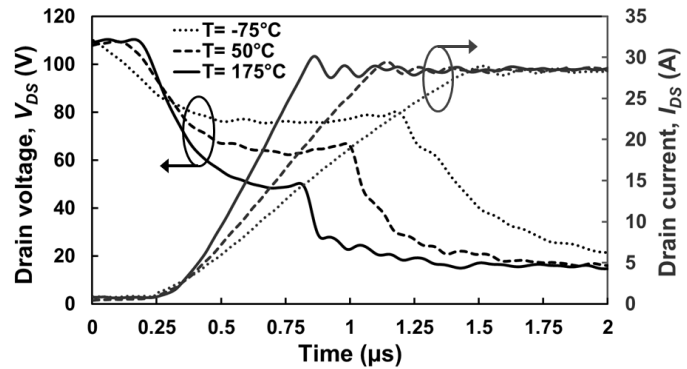
Fig. 10. SiC MOSFET turn-ON voltage and current with an R_G of 150 Ω

Figure 11 shows the turn-ON switching energy as a function of the temperature and switching rate for the silicon IGBT. Unlike the MOSFET, switching energy increases with temperature for all the switching rates. This is due to the bipolar nature of IGBTs and the reverse recovery of the PiN diode. Temperature increases the lifetime of the minority carriers in the conductivity modulation region of the IGBT and PiN diode, hence, the switching duration is prolonged as temperature is increased. Figure 12 and Figure 13 show the voltage and current turn-ON transients in the silicon IGBT at different temperatures with R_G=15 Ω and R_G=150 Ω respectively. For the silicon IGBT, at R_G=10 Ω, the switching energy increases by 10% when the temperature is increased from -75 °C to 175 °C, whereas at R_G=1000 Ω, the switching energy increases by 30% for the same temperature change.
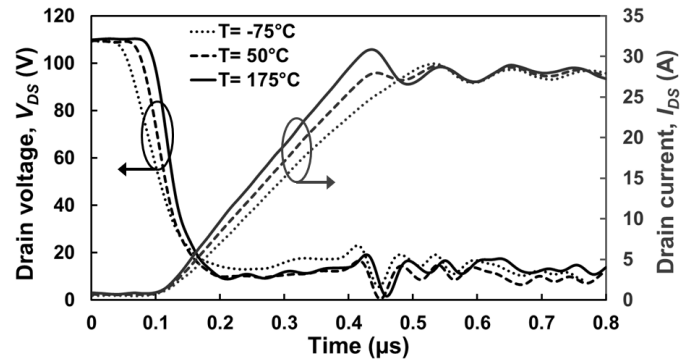

Fig. 11. Switching energy of Silicon IGBT at turn-ON

Fig. 12. Silicon IGBT turn-ON voltage and current with an R_G of 15 Ω

Fig. 13. Silicon IGBT turn-ON voltage and current with an R_G of 150 Ω

Fig. 14. Switching energy of SiC MOSFET at turn-OFF

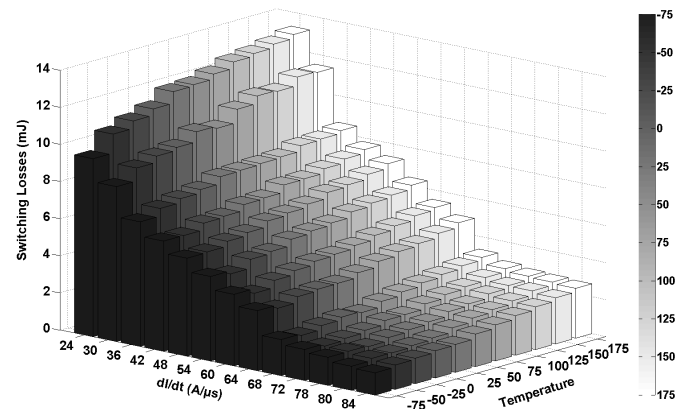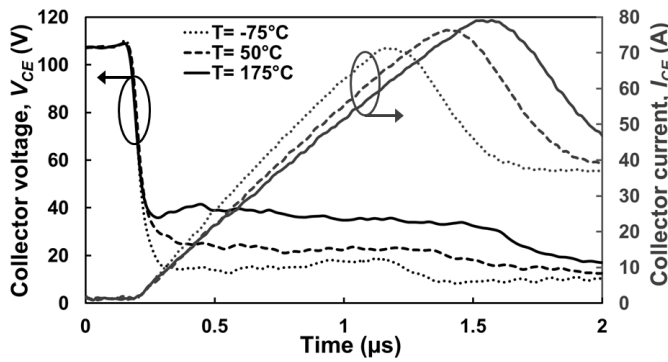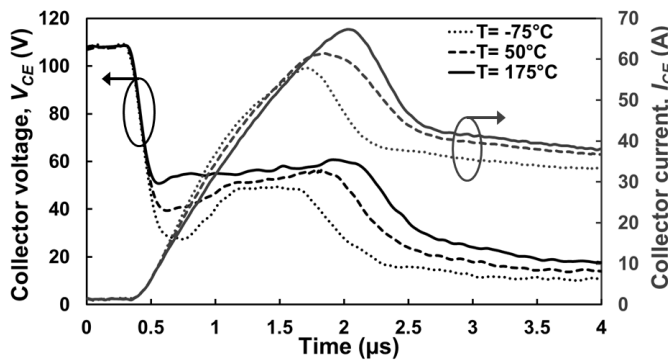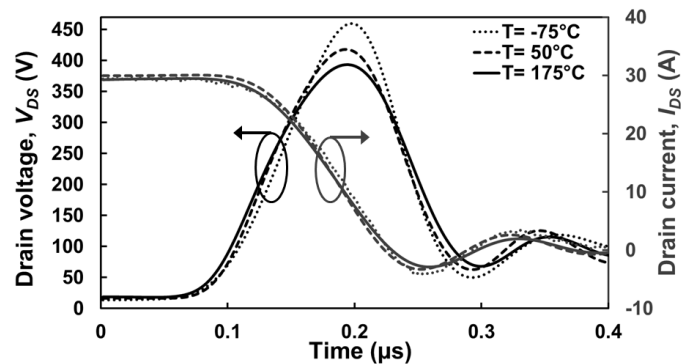Fig. 15. SiC MOSFET turn-OFF voltage and current with an R_G of 15 Ω

Fig. 16. SiC MOSFET turn-OFF voltage and current with an R_G of 150 Ω

B. Transistor Turn-OFF

Figure 14 shows the turn-OFF switching energy of the SiC MOSFET at different temperatures and switching rates. Unlike the turn-ON characteristics, the switching energy increases with temperature during turn-OFF. This trend is due to the fact that dI_{DS}/dt increases with decreasing temperature during turn-OFF which is opposite to the trend during turn-ON. Figure 15 and Figure 16 show transient turn-OFF current and voltage characteristics for the SiC MOSFET with R_G=15 Ω and R_G=150 Ω respectively. It can be seen from Figure 15 and Figure 16 that the currents and voltages switch faster at lower temperatures. This is due to the negative temperature coefficient of the MOSFET's threshold voltage, hence, as the gate is driven from 18 V to zero, the higher threshold voltage of the cold temperature device causes the device to turn-OFF quicker. Also, the peak voltage overshoot in the drain voltage resulting from parasitic inductances is higher when the device is switched faster. In Figure 17 the peak rises to 460 V for R_G=15 Ω and in Figure 16 the peak voltage is 270 V for R_G=150 Ω. It can also be seen that the peak voltage overshoot increases as the temperature decreases as a result of the negative temperature coefficient of dI_{DS}/dt during MOSFET turn-OFF. The switching energy of SiC MOSFET during turn-OFF shows a slight increase with temperature rise [14]. This is due to the fact that oscillations are damped, but the transient duration is also prolonged.

Figure 17 shows the turn-OFF switching energy of the IGBT at different temperatures. The switching energy increases with temperature during turn-OFF because the dI_{CE}/dt at a given R_G increases as temperature increases. Figure 18 and Figure 19 show the V_{CE} and I_{CE} transient characteristics at different temperatures for the IGBT switched with R_G= 15 Ω and R_G= 150 Ω respectively. Similar to the case of turn-OFF in the MOSFET, the IGBT peak V_{CE} overshoot increases as the temperature reduces because of the negative

temperature coefficient of dI_{CE}/dt. As can be seen, the IGBT does not present a significant current tail at turn-OFF. The usual tail current is due to minority carrier recombination in the drift region as the device is turned off and usually increases with temperature because the carrier lifetime has a positive temperature coefficient. The IGBT used in this experiment is a Non-Punch-Through (NPT) type which has been optimized for low switching losses. Because there is no highly doped n+ layer between the voltage blocking drift region and the p+ base, minority carrier injection is not as much as in the punch-through IGBT [15]–[17]. Hence, the absence of the tail current makes the temperature variation more stable.

Fig. 17. Switching energy of the Silicon IGBT at turn-OFF

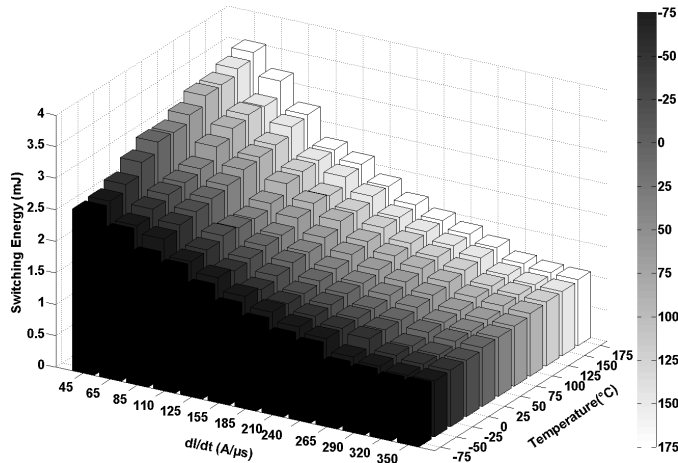Fig. 18. Silicon IGBT turn-OFF voltage and current with an R_G of 15 Ω

Fig. 19. Silicon IGBT turn-OFF voltage and current with an R_G of 150 Ω

C. Diode Turn-ON

Figure 20 shows the turn-ON switching energy of the SiC Schottky diode at different temperatures and MOSFET dI_{DS}/dt. Because the turn-ON of the diode coincides with the turn-OFF of the SiC MOSFET, the dI_{AK}/dt of the current through the diode increases as the temperature reduces. The U-shaped characteristic of the switching energy is due to the trade-off happening between the impact of higher switching rates on oscillations (overshoots, undershoots) and the transient duration. Figures 21 and 22 show the diode turn-ON current and voltage transients for R_G=15 Ω and R_G=150 Ω respectively. It can be seen from Figures 21 and 22 that the dI_{AK}/dt and dV_{AK}/dt increase as the temperature is reduced. It can also be seen that the rate of the increase is higher for the R_G=150 Ω than for the R_G=15 Ω.

Fig. 20. Switching energy of SiC SBD at turn-ON

Fig. 21. SiC SBD at turn-ON voltage and current with an R_G of 15 Ω

Figure 23 shows switching energy of the silicon PiN diodes at different temperatures and different IGBT dI_{DS}/dt during turn-ON. The switching energy increases with the temperature as expected because of the temperature dependent lifetime of the minority carriers in the conductivity modulated region. Figure 24 and Figure 25 show the PiN diode voltage and current transients at different temperatures for R_G=15 Ω and R_G=150 Ω respectively. It can be seen from Figures 24 and 25 that the dI_{AK}/dt increases as the temperature is reduced similar

Fig. 22. SiC SBD at turn-ON voltage and current with an R_G of 150 Ω

Fig. 25. Si PiN diode turn-ON voltage and currents with an R_G of 150 Ω

to the IGBT currents. At high switching rates, the switching energy is dominated by current overshoots whereas at low switching rates, the switching energy is dominated by the transient delay. Hence, each device based on its characteristics, has an optimum point for the *dI/dt* where its switching energy is minimized. As seen in Figure 20, increasing the gate resistance from R_G=15 Ω to R_G=150 Ω has damped the oscillations within the voltage and current waveforms, although prolonging the duration of the switching. This results in a trade-off between the two factors.

D. Diode Turn-OFF

Figure 26 shows the SiC Schottky diode switching energy as a function of temperature and MOSFET dI_{DS}/dt during turn-OFF. Similar to the case of the diode turn-ON, the switching energy exhibits a U shaped characteristic as a function of the MOSFET's dI_{DS}/dt. This happens since at high switching rates, the ringing of the Schottky diode dominates the switching losses while at lower switching rates, the duration of the transient is the dominant cause of increase in switching energies. Figure 27 shows the diode turn-OFF voltage transient as a function of temperature for R_G=15 Ω while Figure 28 shows the same plot for R_G=150 Ω. It can be seen from Figures 27 and 28 that the damping of the diode ringing during turn-OFF reduces with increasing temperature and the peak voltage overshoot increases with temperature i.e. ringing becomes more sustained at high temperatures during diode turn-OFF. This is due to the positive temperature coefficient of the MOSFET turn-ON dI_{DS}/dt, hence, the faster switching at high temperatures contributes to the ringing of the diode. It can also be noticed when comparing Figures 27 and 28 that the temperature dependence of the ringing and the damping reduces at higher MOSFET dI_{DS}/dt (lower R_G) and increases as the dI_{DS}/dt is reduced. i.e. at high dI_{DS}/dt, the diode characteristics become more temperature invariant compared to low dI_{DS}/dt (higher R_G). It can be seen from Figure 28 that there is a significant variation of the V_{AK} transient as the temperature is changed.

Fig. 23. Switching energy of Silicon PiN diode at turn-ON

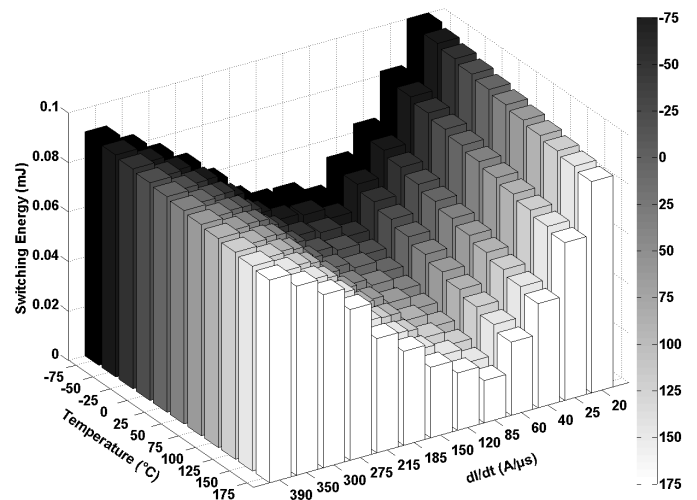Fig. 24. Si PiN diode turn-ON voltage and currents with an R_G of 15 Ω

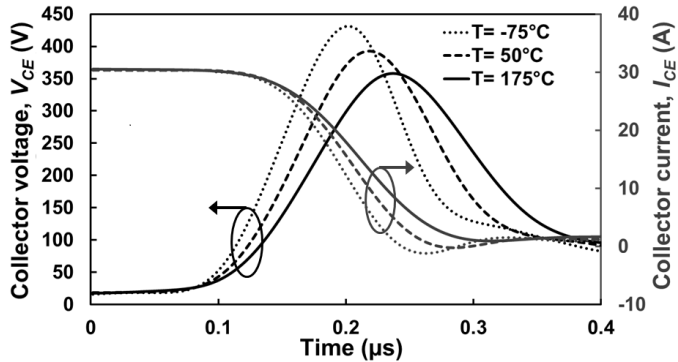Fig. 26. Switching energy of SiC SBD at turn-OFF

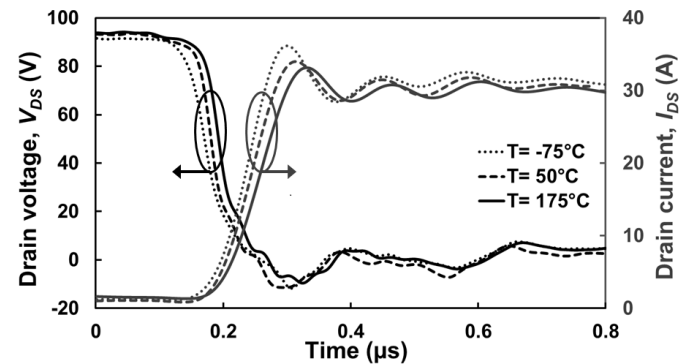Fig. 27.   SiC SBD turn-OFF voltage and currents with an R_G of 15 Ω

Fig. 28.   SiC SBD turn-OFF voltage and currents with an R_G of 150 Ω
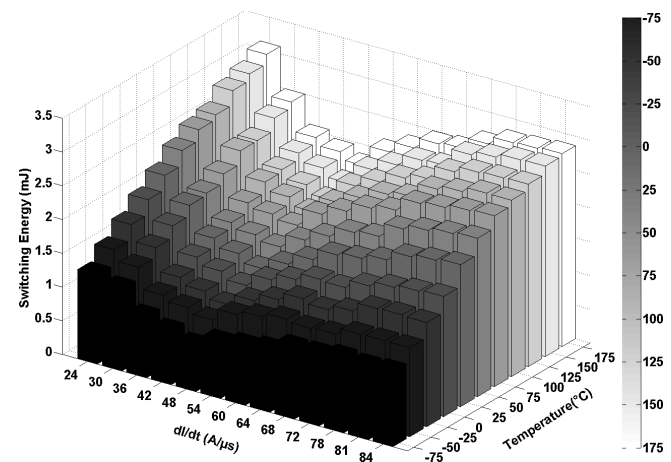
Fig. 29.   Switching energy of Silicon PiN diode at turn-OFF
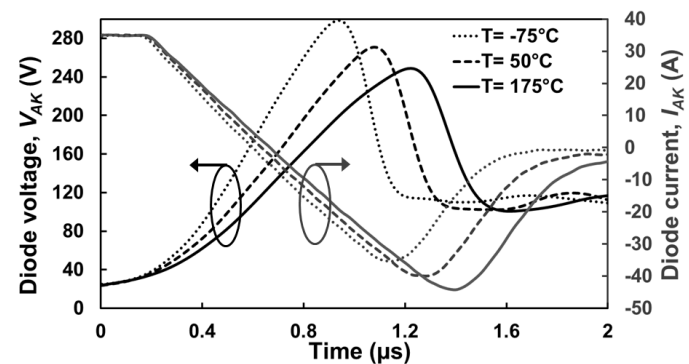
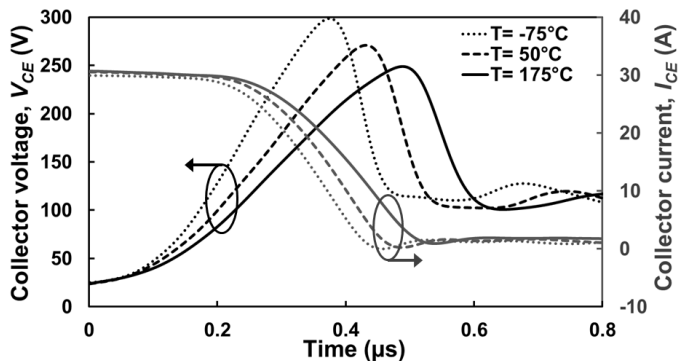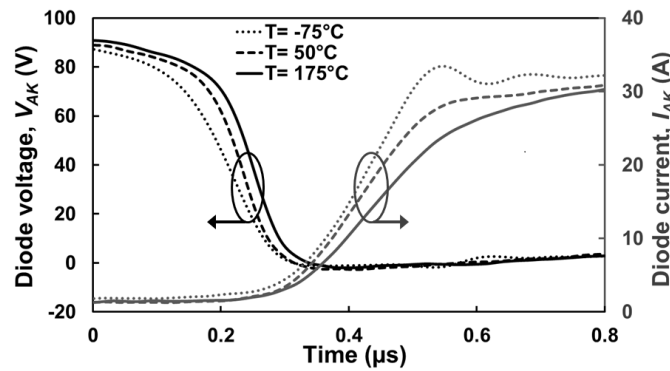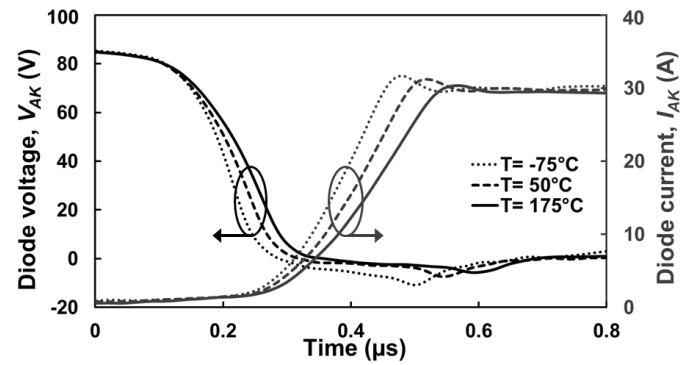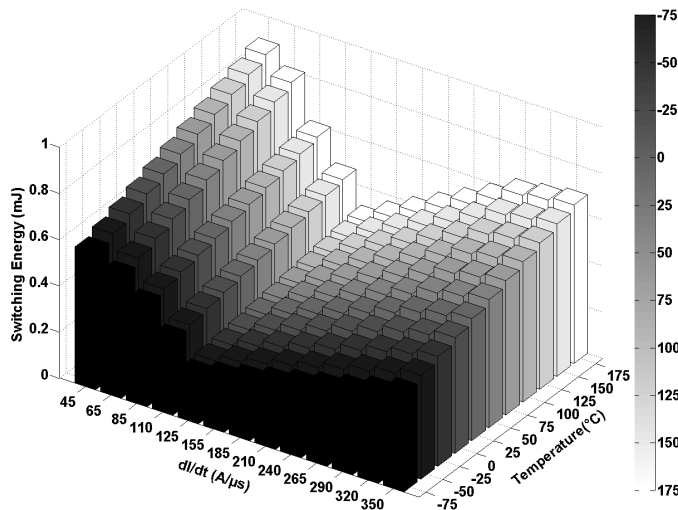Fig. 30.   Si PiN diode turn-OFF voltages and currents with an R_G of 15 Ω

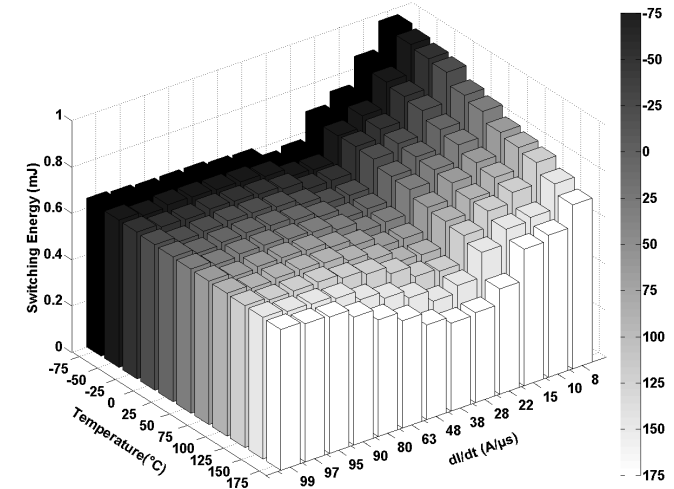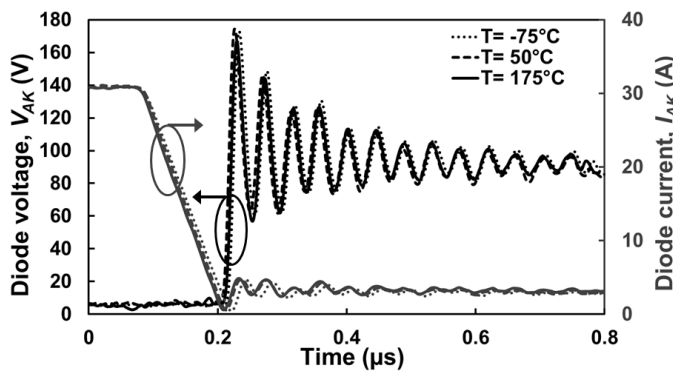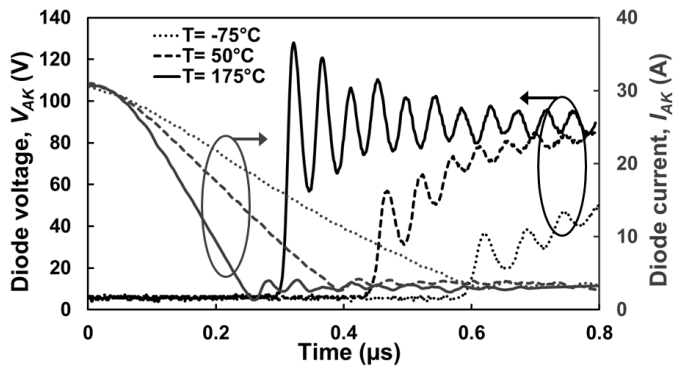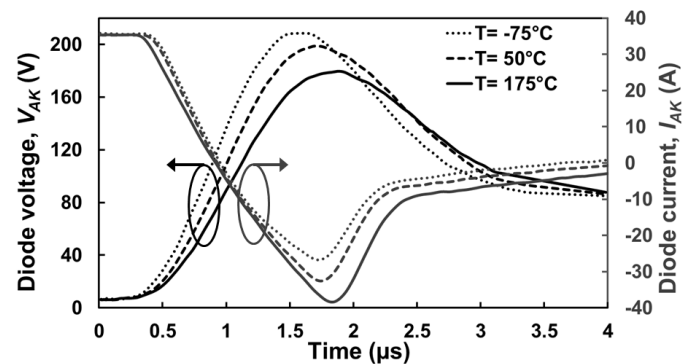

Fig. 31.   Si PiN diode turn-OFF voltages and currents with an R_G of 150 Ω

Figure 29 shows the switching energy of the silicon PiN diode at different temperatures and IGBT dI_{CE}/dt. Figure 30 and Figure 31 shows the PiN diode voltage and current transients for R_G=15 Ω and R_G=150 Ω. It can be seen from Figure 29 that the switching energy increases as the temperature increases for a given R_G or IGBT dI_{CE}/dt. This is due to increased carrier lifetime with temperature thereby increasing the reverse recovery charge of the PiN diode during turn-OFF. Hence, the performance of the PiN diode deteriorates as the temperature increases. It can be seen from Figure 30 and Figure 31 that the peak reverse recovery current increases as R_G is reduced (dI_{CE}/dt is increased) while the transient duration has slightly increased. It can also be observed from Figure 30 and Figure 31 that the peak diode voltage overshoot increases with reducing R_G, hence, fast switching using PiN diodes increases the peak power loss. It can also be seen that the IGBT dI_{CE}/dt increases as temperature is reduced, hence, the peak voltage overshoot (resulting from parasitic inductances) reduces with increasing temperature.

The result of all this is that the switching energy as a function of R_G exhibits a U-shaped characteristic at all temperatures. At low R_G, the switching energy is dominated by high peak reverse recovery currents and large diode voltage overshoots while at higher R_G, the switching energy is dominated by the longer switching duration which results in further increase in switching losses. Figure 32 shows a comparison of the SiC MOSFET and IGBT switching energies as a function of temperature with R_G=15 Ω for both turn-ON and turn-OFF. The SiC MOSFET shows less switching energy

compared with the IGBT. The switching energy also shows less temperature dependency in the SiC MOSFET compared with the IGBT. Figure 33 shows that the switching energy of the SiC Schottky diode is less than that of the PiN diode. Figure 33 also shows that the switching energy of the SiC Schottky diode at turn-OFF has a negative temperature coefficient.

IV. ELECTRIC VEHICLE DRIVE-TRAIN MODEL

The 3-D plots of the transistor and diode switching energy have been used as inputs into a 3-level 3-phase NPC-VSC model in PLECS where the drive-train of the electric vehicle

Fig. 32.   Transistors switching energy as a function of temperature, R_G=15Ω

Fig. 33.   Rectifiers switching energy as a function of temperature, R_G=15Ω

is modeled by connecting the converter output to a 3 phase 8 pole permanent magnet synchronous machine [18]–[20]. The transistor and diode switching energies as functions of the supply voltage, current and temperature were used to parameterize the switching devices. Other input parameters for the converter models were the switching frequency, the ca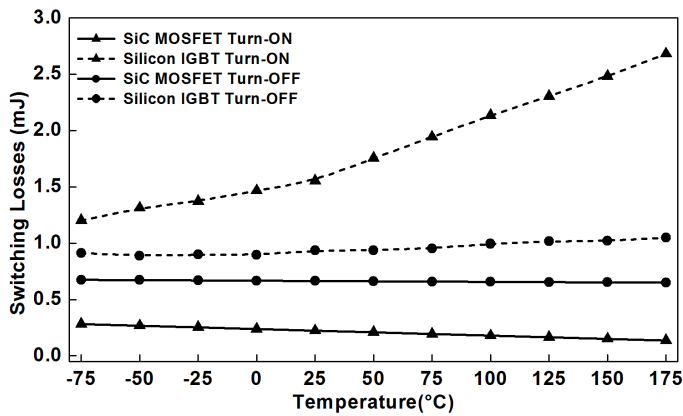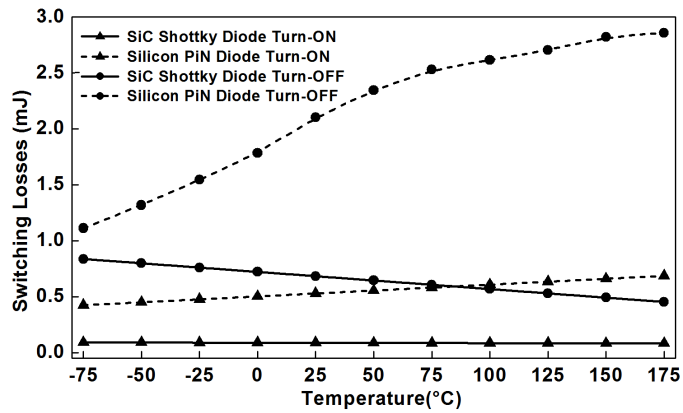lculated turn-ON/OFF time delay (dI_{DS}/dt or dI_{CE}/dt) and the pulse width modulation (PWM) technique. Figure 34 shows the switching energy as functions of the voltage and current of the devices at different temperatures as well as a schematic of the model converter connected to the electrical motor [21]. The switching energy measurements at different temperatures were inserted into a look-up table in the device model and used to determine the performance of the electric drive-train. Hence, depending on the switching frequency and *dI/dt* used in the drive-train, the corresponding switching energy of the device is used to perform the simulation. The rate of change of current with time ((dI_{DS}/dt or dI_{CE}/dt)) is specific to the technology (SiC MOSFET or IGBT). For each switching instance, the device is conducting for 10 times the sum of the turn ON/OFF periods. Figure 35 shows the converter output waveform, before filtering.

Different modulation techniques were used in the models. These include the Sinusoidal PWM (SPWM) [22], saw-tooth PWM [23], space vector PWM (SVPWM) [24], Third Harmonic Injection PWM with 25% of main carrier

(THIPWM(4)) [25], Third Harmonic Injection with a coefficient of 16% of main carrier (THIPWM(6)) [26], Triple Harmonic Injection PWM (TRIPWM) [27], Inverted Sine Carrier PWM (ISCPWM) [28] and Inverted Sine Carrier Third Harmonic Injection PWM (ISCTHIPWM) [29]. These PWM techniques are conventionally used in vehicle applications. Examples may be SPWM, SVPWM and THIPWM [30]. The thermal parameters (thermal resistance and thermal capacitance) of the heat sink in the models was selected on the basis of published thermal parameters for commercial heat-sinks and are used as input into the converters thermal model. The thermal impedances of the devices were obtained from the datasheets and were also used as inputs into the thermal model. Also the thermal impedance of devices are implemented in the model as a cauer type through their datasheets. Figure 36 shows the steady state temperature rise of the converter for the different PWM techniques with the carrier frequency at 5 kHz and the gate resistance at 15 Ω. The SiC MOSFET and silicon IGBT were distinguished in the model by different turn-ON/OFF delays that were experimentally measured for gate resistances.
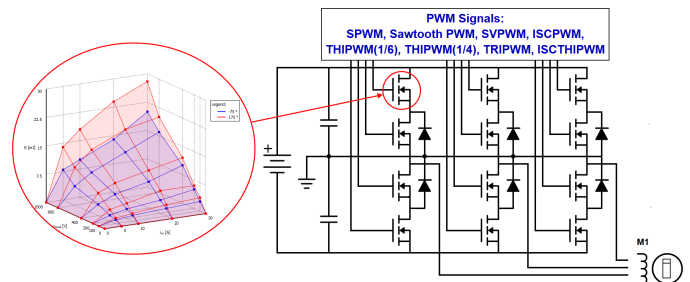

Fig. 34.   Topology of the 3-level NPC VSC and the 8 pole PMSM; the heatsink although not shown, is connected to all transistors and rectifiers with parameters described in Table I.
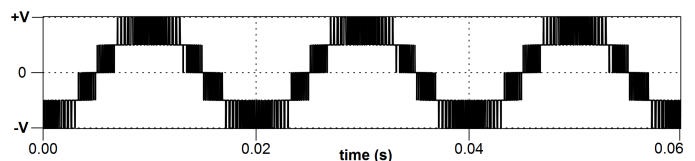

Fig. 35.   Output voltage waveform of the 3-Level NPC VSC model before filtering.
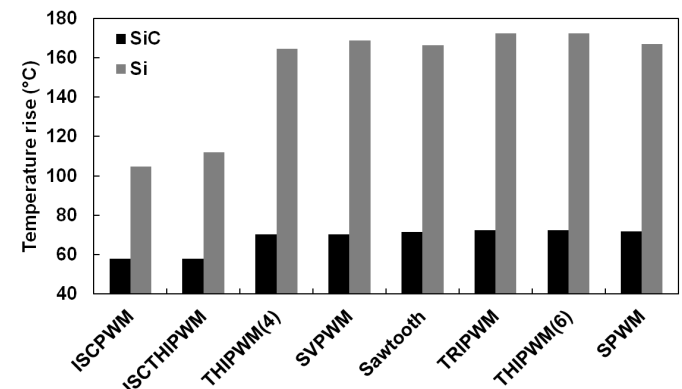

Fig. 36.   Modelled temperature rise of the VSC with different PWM techniques, R_G of 15 Ω and 5 kHz carrier frequency.

The smaller switching energy of the SiC MOSFET is translated into a smaller temperature rise compared with the IGBT as can be seen in Figure 36 . The conversion efficiency of the VSC is also calculated by determining the ratio of the power losses to input power. The conversion efficiency is simply the effect of the losses on the reduction of the output energy compared to the input one. Hence, the switching energy of devices in each cycle compared to the input power shows how much energy is lost due to switching transients. The results are shown in Figure 37 where the conversion efficiency is calculated for the different PWM techniques for both technologies, although the quality of the conversion output is not taken into account here. It clearly shows that the SiC devices outperform the silicon devices in terms of conversion efficiency by at least 1.8% as a result of smaller switching energies.
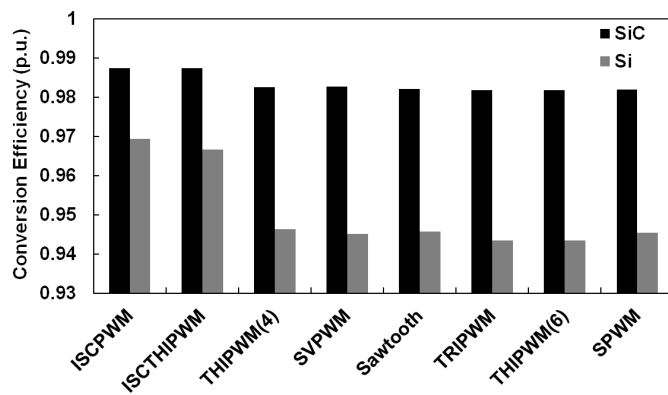

Fig. 37.   Modelled conversion efficiency of the 3-Level NPC VSC with different PWM techniques, R_G of 15 Ω and 5kHz carrier frequency.

The impact of changing the R_G (hence dI_{DS}/dt for the MOSFET and dI_{CE}/dt for the IGBT) and the switching frequency on the temperature rise in the converter is also modeled for both technologies. Changing the switching frequency will impact the THD, the temperature rise as well as the reliability of the converter. Faster switching is usually desirable in 2 or 3 level converters because it can reduce the filtering requirements needed by the converters output. Figure 38 shows the converter temperature and motor speed (in rpm) of the drive-train as a function of time for the converter modeled with SiC MOSFET and silicon IGBT switching parameters. The carrier frequency in the PWM modulation is kept at 60 Hz while the modulation frequency is ranged between 5 kHz and 15 kHz. The final motor speed attained is 900 rpm through Carrier Based Space Vector Pulse Width Modulation. Figure 38 shows that increasing the PWM switching frequency from 5 kHz to 15 kHz increases the operating temperature of the converter by 72% for the silicon IGBT converter and 50% for the SiC MOSFET converter. However, at 15 kHz and 5 kHz, the steady state operating temperature of the modeled SiC converter is 53% and 50% lower than that of the modelled silicon IGBT converter. This reduction of the operating temperature can lead to simpler cooling systems, more efficient and compact electric vehicle drive-trains as well as better device reliability since

the reliability is usually strongly affected by temperature. Figure 39 shows the model's results of the SiC MOSFET and silicon IGBT converters with 2 different gate resistances used (R_G=15 Ω and R_G=150 Ω). The gate resistance used will determine the maximum possible switching frequency and will also determine the electromagnetic oscillations in the output characteristics of the devices. Figure 39 shows that the converter modeled with SiC MOSFETs exhibits a smaller temperature rise as a result of the smaller switching energy. What can also be observed in Figure 39 is the fact that increasing the gate resistance for slower switching increases the temperature rise as a result of the increased switching energy. It is sometimes desirable to slightly increase the gate resistance so as to reduce the electromagnetic stresses imposed on the device i.e. fast switching can cause oscillations in output characteristics as seen with the Schottky diodes as they can have an adverse effect on reliability and electromagnetic emissions [31]. The THD of the 3 phase output of the converter was also estimated in the model as a function of the technology. It is known that increasing the switching frequency will shift the higher amplitude harmonics to higher frequencies, hence making them easier to filter. However, this will come at the expense of increased switching losses and higher operating temperature as shown in Figure 38. The use of SiC can nevertheless relax this trade-off since the temperature rise associated with faster switching is less for SiC unipolar compared with silicon bipolar technologies. This is clearly advantageous in applications where weight or size of passives is critical like off-shore wind turbines [32] or aviation [33].
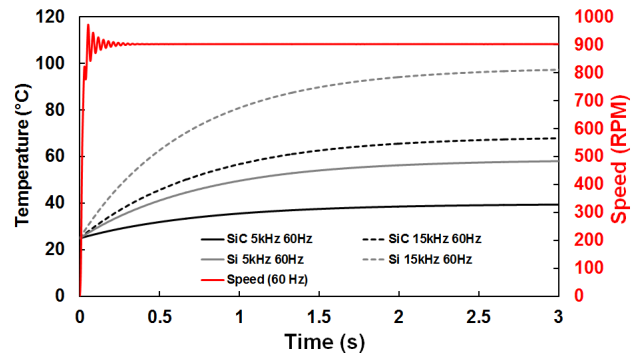

Fig. 38.   Effect of switching frequency variation on the temperature rise of Si/SiC based 3-level NPC VSC on a CB-SVPWM drive with R_G of 15 Ω.
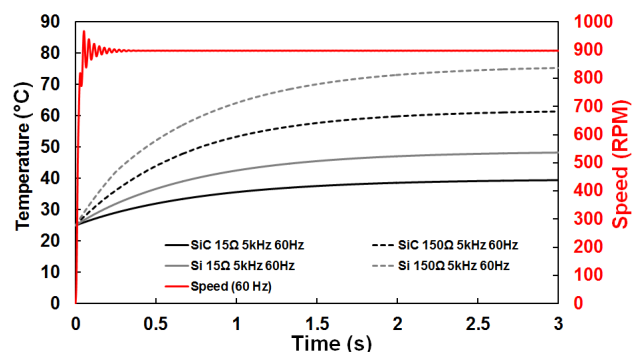

Fig. 39.   Effect of R_G variation on the temperature rise of Si/SiC based 3-level NPC VSC on a CB-SVPWM drive with a carrier frequency of 5kHz.

V. CONCLUSION

This paper has explored the impact of wide bandgap technology on energy conversion for EVs through model of EV drive-trains and experimental measurements of SiC unipolar and silicon bipolar power devices. The temperature dependency of the switching energy in SiC MOSFETs/Schottky diode pairs have been compared to that of silicon IGBT/PiN diode pairs. The switching energy was experimentally measured for 1.2kV devices for a temperature range between -75 °C and 175 °C using a range of gate resistances to vary *dI/dt* and switching rates of the transients. The switching rates (dI_{DS}/dt for the Unipolar and dI_{CE}/dt for the Bipolar) were shown to be temperature dependent with the SiC MOSFET switching rate showing a negative temperature coefficient at turn-ON and a positive temperature coefficient at turn-OFF. The IGBT switching rates increased with temperature for both turn-ON and turn-OFF. The switching energy of the SiC MOSFET has been shown to decrease with temperature whereas that of the silicon IGBT increases.

The switching energy of the diodes generally shows a U-shaped characteristic as a function of the gate resistances. At small gate resistances, the switching energy of the PiN diodes is dominated by the peak reverse recovery charge in the drift region and high diode voltage overshoots. In SiC diodes, the switching energy at small gate resistances is dominated by diode ringing. The electric vehicle drive-train model which consisted of a permanent magnet synchronous machine connected to the output of 3-level 3-phase NPC-VSC showed significant improvements when the model is parameterized with SiC MOSFET measurements compared with silicon IGBT measurements. The VSC model with SiC parameters exhibited less operating temperatures compared with silicon IGBTs at the same switching frequency thus implying a reduction of cooling requirements. Also, the VSC model with SiC MOSFETs exhibited smaller steady state temperature excursions while running at twice the switching frequency compared with silicon IGBT VSCs thereby signifying that energy density can be increased significantly with SiC technology. SiC VSC models also show slightly smaller THD at a given switching frequency due to the device's higher switching rate. SiC technology can therefore improve the operation of VSCs in terms of cooling requirements, energy density and THD all of which contribute significantly to the efficiency and performance of electric vehicles.

REFERENCES

[1] J. Estima and A. Marques Cardoso, "Efficiency analysis of drive train topologies applied to electric/hybrid vehicles," *Vehicular Technology, IEEE Transactions on*, vol. 61, no. 3, pp. 1021–1031, March 2012.

[2] J. Hudgins, "Power electronic devices in the future," *Emerging and Selected Topics in Power Electronics, IEEE Journal of*, vol. 1, no. 1, pp. 11–17, March 2013.

[3] A. Merkert, T. Krone, and A. Mertens, "Characterization and scalable modeling of power semiconductors for optimized design of traction inverters with si- and sic-devices," *Power Electronics, IEEE Transactions on*, vol. 29, no. 5, pp. 2238–2245, May 2014.

[4] J. Biela, M. Schweizer, S. Waffler, and J. Kolar, "Sic versus sievaluation of potentials for performance improvement of inverter and dcdc converter systems by sic power semiconductors," *Industrial Electronics, IEEE Transactions on*, vol. 58, no. 7, pp. 2872–2882, July 2011.

[5] R. S. Howell, S. Buchoff, S. Van Campen, T. R. McNutt, A. Ezis, B. Nechay, C. Kirby, M. Sherwin, R. Clarke, and R. Singh, "A 10-kv large-area 4h-sic power dmosfet with stable subthreshold behavior independent of temperature," *Electron Devices, IEEE Transactions on*, vol. 55, no. 8, pp. 1807–1815, Aug 2008.

[6] J. Wang, X. Zhou, J. Li, T. Zhao, A. Huang, R. Callanan, F. Husna, and A. Agarwal, "10-kv sic mosfet-based boost converter," *Industry Applications, IEEE Transactions on*, vol. 45, no. 6, pp. 2056–2063, Nov 2009.

[7] T. Salem and R. Wood, "1000-h evaluation of a 1200-v, 880-a all-sic dual module," *Power Electronics, IEEE Transactions on*, vol. 29, no. 5, pp. 2192–2198, May 2014.

[8] H. Zhang and L. Tolbert, "Efficiency impact of silicon carbide power electronics for modern wind turbine full scale frequency converter," *Industrial Electronics, IEEE Transactions on*, vol. 58, no. 1, pp. 21–28, Jan 2011.

[9] M. Nymand and M. A. E. Andersen, "High-efficiency isolated boost dcdc converter for high-power low-voltage fuel-cell applications,," *Industrial Electronics, IEEE Transactions on*, vol. 57, no. 2, pp. 505–514, Feb 2010.

[10] B. Ozpineci, M. Chinthavali, L. Tolbert, A. Kashyap, and H. Mantooth, "A 55 kw three-phase inverter with si igbts and sic schottky diodes," in *Applied Power Electronics Conference and Exposition, 2006. APEC '06. Twenty-First Annual IEEE*, March 2006, pp. 7 pp.–.

[11] H. Zhang, L. Tolbert, and B. Ozpineci, "Impact of sic devices on hybrid electric and plug-in hybrid electric vehicles," *Industry Applications, IEEE Transactions on*, vol. 47, no. 2, pp. 912–921, March 2011.

[12] B. Whitaker, A. Barkley, Z. Cole, B. Passmore, D. Martin, T. McNutt, A. Lostetter, J. S. Lee, and K. Shiozaki, "A high-density, high-efficiency, isolated on-board vehicle battery charger utilizing silicon carbide power devices," *Power Electronics, IEEE Transactions on*, vol. 29, no. 5, pp. 2606–2617, May 2014.

[13] J.-S. Lai, B.-M. Song, R. Zhou, J. Hefner, A., D. Berning, and C.-C. Shen, "Characteristics and utilization of a new class of low on-resistance mos-gated power device," *Industry Applications, IEEE Transactions on*, vol. 37, no. 5, pp. 1282–1289, Sep 2001.

[14] K. Sun, H. Wu, J. Lu, Y. Xing, and L. Huang, "Improved modeling of medium voltage sic mosfet within wide temperature range," *Power Electronics, IEEE Transactions on*, vol. 29, no. 5, pp. 2229–2237, May 2014.

[15] F. Calmon, S. Lefebvre, J.-p. Chante, D. Ligot, and B. Reymond, "Thermal behaviour of pt and npt igbt," in *Power Electronics and Variable-Speed Drives, 1994. Fifth International Conference on*, Oct 1994, pp. 29–34.

[16] S. Azzopardi, C. Jamet, J. M. Vinassa, and C. Zardini, "Switching performances comparison of 1200 v punch-through and nonpunch-through igbts under hard-switching at high temperature," in *Power Electronics Specialists Conference, 1998. PESC 98 Record. 29th Annual IEEE*, vol. 2, May 1998, pp. 1201–1207 vol.2.

[17] K. Sheng, B. Williams, and S. Finney, "Maximum operating junction temperature of pt and npt igbts," *Electronics Letters*, vol. 34, no. 23, pp. 2276–2277, Nov 1998.

[18] J. Schonberger, "Averaging methods for electrical-thermal converter models," in *Power Electronics and Applications (EPE 2011), Proceedings of the 2011-14th European Conference on*, Aug 2011, pp. 1–8.

[19] G. Pellegrino, A. Vagati, P. Guglielmi, and B. Boazzo, "Performance comparison between surface-mounted and interior pm motor drives for electric vehicle application," *Industrial Electronics, IEEE Transactions on*, vol. 59, no. 2, pp. 803–811, Feb 2012.

[20] K. Rajashekara, "Present status and future trends in electric vehicle propulsion technologies," *Emerging and Selected Topics in Power Electronics, IEEE Journal of*, vol. 1, no. 1, pp. 3–10, March 2013.

[21] D. Andler, R. Alvarez, S. Bernet, and J. Rodriguez, "Switching loss analysis of 4.5-kv5.5-ka igcts within a 3l-anpc phase leg prototype,," *Industry Applications, IEEE Transactions on*, vol. 50, no. 1, pp. 584–592, Jan 2014.

[22] Z. Zhao, J.-S. Lai, and Y. Cho, "Dual-mode double-carrier-based sinusoidal pulse width modulation inverter with adaptive smooth transition control between modes," *Industrial Electronics, IEEE Transactions on*, vol. 60, no. 5, pp. 2094–2103, May 2013.

[23] H. Mouton and B. Putzeys, "Understanding the pwm nonlinearity: Single-sided modulation," *Power Electronics, IEEE Transactions on*, vol. 27, no. 4, pp. 2116–2128, April 2012.

[24] C. Xia, H. Shao, Y. Zhang, and X. He, "Adjustable proportional hybrid svpwm strategy for neutral-point-clamped three-level inverters,"

Industrial Electronics, IEEE Transactions on, vol. 60, no. 10, pp. 4234–4242, Oct 2013.

[25] A. Hava, R. Kerkman, and T. Lipo, "A high-performance generalized discontinuous pwm algorithm," *Industry Applications, IEEE Transactions on*, vol. 34, no. 5, pp. 1059–1071, Sep 1998.

[26] D. Holmes and B. McGrath, "Opportunities for harmonic cancellation with carrier-based pwm for a two-level and multilevel cascaded inverters," *Industry Applications, IEEE Transactions on*, vol. 37, no. 2, pp. 574–582, Mar 2001.

[27] C. Aghion, O. Ursaru, M. Lucanu, C. Pavaluta, and O. Botez, "Motor control strategy based on iscpwm and thipwm," in *Signals, Circuits and Systems (ISSCS), 2011 10th International Symposium on*, June 2011, pp. 1–4.

[28] R. Nandhakumar and S. Jeevananthan, "Inverted sine carrier pulse width modulation for fundamental fortification in dc-ac converters," in *Power Electronics and Drive Systems, 2007. PEDS '07. 7th International Conference on*, Nov 2007, pp. 1028–1034.

[29] C. Navabalachandru, B. Ashok, A. Jagadeesan, and R. Raja, "Performance of variable frequency ispwm technique for a cascaded multilevel inverter," in *Energy Efficient Technologies for Sustainability (ICEETS), 2013 International Conference on*, April 2013, pp. 611–616.

[30] H. Wen, W. Xiao, X. Wen, and P. Armstrong, "Analysis and evaluation of dc-link capacitors for high-power-density electric vehicle drive systems," *Vehicular Technology, IEEE Transactions on*, vol. 61, no. 7, pp. 2950–2964, Sept 2012.

[31] N. Idir, R. Bausiere, and J. Franchaud, "Active gate voltage control of turn-on di/dt and turn-off dv/dt in insulated gate transistors," *Power Electronics, IEEE Transactions on*, vol. 21, no. 4, pp. 849–855, July 2006.

[32] I. Girsang, J. Dhupia, E. Muljadi, M. Singh, and J. Jonkman, "Modeling and control to mitigate resonant load in variable-speed wind turbine drivetrain," *Emerging and Selected Topics in Power Electronics, IEEE Journal of*, vol. 1, no. 4, pp. 277–286, Dec 2013.

[33] S. Motapon, L.-A. Dessaint, and K. Al-Haddad, "A comparative study of energy management schemes for a fuel-cell hybrid emergency power system of more-electric aircraft," *Industrial Electronics, IEEE Transactions on*, vol. 61, no. 3, pp. 1320–1334, March 2014.

Craig Fisher was born in Warwickshire, UK, in 1984. He received the M.Sc. degree in Advanced Electronics Engineering from the University of Warwick, UK in 2010, and is currently studying towards the Ph.D. degree in the field of silicon carbide power electronics, also from the University of Warwick. This Ph.D. is funded by the EPSRC HubNet project, and has focused on three principle areas: novel edge termination solutions for high voltage power devices, carrier lifetime enhancement using high temperature processes and the formation of robust ohmic contacts to p-type 4H-SiC. His research interests include modelling of 4H-SiC power devices, and the fabrication and characterisation of 4H-SiC devices for high voltage (>10 kV) and high temperature (>300 °C) applications.

Li Ran (M'98-SM'07) received a PhD degree in Power Systems Engineering from Chongqing University, Chongqing, China, in 1989. He was a Research Associate with the Universities of Aberdeen, Nottingham and Heriot-Watt, at Aberdeen, Nottingham and Edinburgh in the UK respectively. He became a Lecturer in Power Electronics with Northumbria University, Newcastle upon Tyne, the UK in 1999 and was seconded to Alstom Power Conversion, Kidsgrove, the UK in 2001. Between 2003 and 2012, he was with Durham University, Durham, the UK. He joined the University of Warwick, Coventry, the UK as a Professor in Power Electronics - Systems in 2012. His research interests include the application of Power Electronics for electric power generation, delivery and utilisation.

Saeed Jahdi (M'10) received the BSc degree in Electrical Power Engineering from University of Science and Technology, Tehran, Iran, in 2005 and the MSc degree with distinction in Power Systems and Energy Management from City University London, U.K., in 2012. Since then, he is pursuing the Ph.D. degree in electrical engineering as a candidate in Power Electronics laboratory of School of Engineering of University of Warwick, U.K. while he has been awarded an energy theme scholarship for the duration of his research. His current research interests include wide band-gap semiconductor devices in high voltage power converters, circuits, testing and applications. Mr. Jahdi is a member of IEEE Power Electronics and Industrial Electronics societies.

Olayiwola Alatise received the B.Eng. degree (with first-class honors) in electrical and electronic engineering and the Ph.D. degree in microelectronics and semiconductors from Newcastle University, Newcastle upon Tyne, U.K., in 2008. His research focused on mixed-signal performance enhancements in strained Si/SiGe metaloxidesemiconductor field-effect transistors (MOSFETs). In 2004 and 2005, he briefly joined Atmel North Tyneside, where he worked on the process integration of the 130-nm CMOS technology node. In June 2008, he joined the Innovation R&D Department, NXP Semiconductors, as a Development Engineer, where he designed, processed, and qualified discrete power trench MOSFETs for automotive applications and switched-mode power supplies. In November 2010, he became a Science City Research Fellow with the University of Warwick and since August 2012, he is serving as assistant professor of Electrical Engineering in University of Warwick, Coventry, U.K. His research interest include investigating advanced power semiconductor materials and devices for improved energy conversion efficiency. Dr. Alatise is a member of IEEE and IET.

Philip Mawby (S'85-M'86-SM'01) received the B.Sc. and Ph.D. degrees in electronic and electrical engineering from the University of Leeds, Leeds, U.K., in 1983 and 1987, respectively. His Ph.D. thesis was focused on GaAs/AlGaAs heterojunction bipolar transistors for high-power radio frequency applications at the GEC Hirst Research Centre, Wembley, U.K.

In 2005, he joined the University of Warwick, Coventry, U.K., as the Chair of power electronics. He was also with the University of Wales, Swansea, U.K. for 19 years and held the Royal Academy of Engineering Chair for power electronics, where he established the Power Electronics Design Center, which has been involved in a whole range of areas relating to power electronics and interaction with small and medium enterprises (SMEs) in Wales as well as larger international companies. He has been internationally recognized in the area of power electronics and power device research. He was also involved in the development of device simulation algorithms, as well as optoelectronic and quantum-based device structures. He has authored or coauthored more than 70 journal papers and 100 conference papers. His current research interests include materials for new power devices, modeling of power devices and circuits, and power integrated circuits.

Prof. Mawby has been involved in many international conference committees, including the International Symposium on Power Semiconductor Devices, the European Power Electronics, the Bipolar/BiCMOS Circuits and Technology Meeting, and the European Solid-State Device Research Conference. He is a Chartered Engineer, a Fellow of the Institution of Engineering and Technology, and a Fellow of the Institute Physics. He is a Distinguished Lecturer for the IEEE Electron Devices Society.